Pion correlations in 1.8 A GeV Ar on KCl and La and 1.2 A GeV Xe on La

W. B. Christie
University of California, Davis, Davis, California 95616
and Lawrence Berkeley Laboratory, Berkeley, California 94720

W. F. J. Mueller, D. L. Olson, T. J. M. Symons, and H. H. Wieman
Nuclear Science Division, Lawrence Berkeley Laboratory, Berkeley, California 94720

D. Beavis
Brookhaven National Laboratory, Upton, New York 11973

F. P. Brady, J. L. Romero, and C. E. Tull
University of California, Davis, Davis, California 95616

T. Abbott and S. Y. Fung
University of California, Riverside, California 92521

D. Keane
Kent State University, Kent, Ohio 44242

Y. Liu
Harbin Institute of Technology, People's Republic of China
(Received 10 February 1992)

Results are presented for pion interferometry measurements of 1.8 A GeV Ar+KCl and Ar+La, and 1.2 A GeV Xe + La at the Lawrence Berkeley Laboratory Heavy Ion Spectrometer System. The parameters R, τ, λ, $R_\perp$, and $R_\parallel$ are presented for all three projectile-target combinations. The correlation between the extracted size of the pion source and the centrality of the collision is investigated as well as the freeze-out densities and the dependence of the source size on the mean momentum of the pion pairs. The experimental setup and analysis are discussed and comparisons made with the results of others. The phase space covered is at forward angles in the center-of-mass system.

PACS number(s): 25.75.+r

INTRODUCTION

Relativistic heavy-ion collisions have been studied in experiments at the Lawrence Berkeley Laboratory BEVALAC for almost twenty years [1]. One of the primary interests in these studies has been to investigate how nuclear matter behaves at the high temperatures and pressures achieved in these collisions. As one cannot solve directly the many-body problems present in analyzing these heavy-ion collisions, the approach taken by many theorists in this area of study is to describe these reactions in the language of thermodynamics. This being the case, one then talks about investigating the equation of state of the nuclear matter in these collisions, and measuring such parameters as the pressure, temperature, volume, entropy, etc. [1].

A simple geometric model is usually used when describing high energy nucleus-nucleus collisions. In this model [2–4], commonly referred to as abrasion ablation or participant spectator, when the two nuclei collide the overlap regions of the two nuclei interact with one another, forming a hot, dense, interaction region, while the remaining parts of the projectile and target nuclei are left largely unaffected aside from some excitation energy. It is this interaction region which we wish to study.

As the pions that come out of these collisions are created in the interaction region of these collisions, they are a natural probe to use in the study of the overlap region.

To extract some measure of the volume of the interaction region, and, if one knows the number of participants, the density, one may use the correlations of identical particles [5–12]. This technique, commonly referred to as the Goldhaber-Goldhaber-Lee-Pais (GGLP) or Hanbury-Brown–Twiss (HBT) technique, and its application to a few different projectile-target combinations is the subject of this article. In addition to, and many would say more interesting than, the space-time extension of the pion source, there are theories which indicate that one may be able to use the magnitude of the pion correlation effect to extract information on the degree of coherence of the pion source. More complete details for this experiment may be found in Ref. [13].

Experimental evidence for the existence of correlations in particle momenta in high energy collisions due to the type of statistics the particles obey, either Fermi-Dirac or Bose-Einstein, was first reported about thirty years ago.

In order to extract meaningful information from a particle correlation analysis, two general categories of questions require particular attention. These categories are the following: (1) What other processes distort the particles momenta, in this case negative pions, coming from the nuclear collisions, by how much are they distorted, and how will it show up in the analysis? (2) What quantities is one actually measuring?

Intensity interferometry

The first experimental evidence that some measure of the size of the pion source could be obtained from the phase space density of the emitted pions momenta was obtained by Goldhaber [14] *et al.* (GGLP effect) while analyzing $\bar{p}$-p annihilations in the late 1950s.

In the early 1970s a number of theorists [6–12], at roughly the same time, realized that the GGLP effect was analogous to the HBT effect [5] in radio and optical astronomy. This lead to a much more straightforward technique of analyzing the data to extract the space-time information for the pion source.

The derivation of the pion correlation can be found in many papers [9,10,15]. What one finds is that for two identical bosons the correlation function is given by

$$C_2(q,q_0)\equiv 1+|\rho(q,q_0|^2 , \tag{1}$$

where $q=|p_1-p_2|$ is the relative three-momentum, $q_0=|E_1-E_2|$, and $\rho(q,q_0)$ is the Fourier transform of the pion emitting source distribution. To continue, one must make some assumption for the form of this distribution. Following the work of Yano and Koonin [10] we have chosen to use their Gaussian distribution for the spatial and temporal distribution. This distribution is parametrized as

$$\rho(r_\perp,r_\parallel,t)=\frac{1}{\pi^2 R^3 \tau}e^{(-r_\perp^2/R_\perp^2-r_\parallel^2/R_\parallel^2-t^2/\tau^2)} \tag{2}$$

or, with the assumption that $R_\perp=R_\parallel$, as

$$\rho(r,t)=\frac{1}{\pi^2 R^3 \tau}e^{(-r^2/R^2-t^2/\tau^2)} . \tag{3}$$

$R_\perp$ and $R_\parallel$ above refer to the directions transverse to and parallel to the beam, respectively. Using this form for $\rho(r,t)$ leads to

$$C_2(q,q_0)=1+e^{(-q^2R^2/2-q_0^2\tau^2/2)} . \tag{4}$$

Notice that the expression for C_2 above goes to the value of two as q and q_0 both go to zero. This is merely due to the property of bosons that the probability of a boson going into a state is twice as large if there is already a boson in the state. In practice it has been observed that the experimentally determined correlation very seldom reaches the value of two at the origin. To get a better fit to the data it was first suggested by Deutschmann *et al.* [16] that one put another fit parameter in front of the exponent in the function above. This parameter, typically given the symbol lambda, is usually referred to as the chaoticity or coherence parameter. It allows for a decrease in the magnitude of the two-pion enhancement due to partial coherence of the emitted pions as well as other physical processes [17] acting on the pions. Our final two-pion correlation function is thus

$$C_2(q,q_0)=1+\lambda e^{(-q^2R^2/2-q_0^2\tau^2/2)} \tag{5}$$

or

$$C_2(q,q_0)=1+\lambda e^{(-q_\perp^2R_\perp^2/2-q_\parallel^2R_\parallel^2/2-q_0^2\tau^2/2)} \tag{6}$$

the choice of form depending on whether one assumes the source is spherical.

Experimental extraction of correlation function

The theoretical two-pion correlation function is defined as the normalized ratio of the inclusive two-pion cross section to the product of the single-pion cross sections [11]. While this gives an exact definition of the correlation function it is not the function which is actually fit to the data. Experimentally one extracts a quantity which is the pion pair distribution as a function of q and q_0, or some other parameters related to the pions separation in phase space, for pairs formed from the same event, in which one expects to see the enhancement in the distribution due to the Bose statistics, and divides this by the same distribution for pion pairs, formed using pions from different events, in which one expects most effects *except* those due to the Bose statistics. We will refer to those pairs in which one expects the correlation to manifest itself as correlated pairs, and those in which one does not expect the effect as uncorrelated pairs.

The technique which was employed in this analysis to form the uncorrelated pairs is most commonly known as *event mixing*. With this scheme one forms the uncorrelated background pairs by mixing pions from different events. It is clear that with this method most of the hardware and software acceptances are automatically taken into account, i.e., one can only use negative pions which have come out of the analysis. When using this method one must take great care to use as close to the same type of events as possible in forming the correlated and uncorrelated pairs. In this analysis care has been taken to use exactly the same set of pions in both the correlated and uncorrelated pion pairs.

What may seem at first to be a problem with this method, namely, the conservation of energy, momentum, charge, and various conserved quantum numbers turns out not to be of concern in relativistic heavy-ion collisions. The reason is that the two colliding nuclei supply a large reservoir of energy and quantum numbers of which the detected pions have but a small portion, thus one does not expect any significant kinematic correlations to affect the results.

We close this section with a few general remarks that may answer some common questions concerning particle correlation studies. The first point is that while most processes that are measured in nuclear experiments are the results of, and explained in terms of, either kinematics or dynamics, the basis of Bose-Einstein correlations is *neither*. The bunching in phase space which one investi-

gates in these studies is due solely to the quantum statistics which apply to the particles being studied [12]. Any correlations due to kinematics or dynamics represent the systematic distortions in these analyses, which one hopes to understand and correct for.

The other point which may lead to confusion is the analogy that is often made between the correlations of photons used by Hanbury-Brown and Twiss to measure stellar radii, and the correlations, in this case of negative pions, used to obtain some measure of the spatial and temporal extent of a nuclear collision. As pointed out by Cocconi [8], whereas in the case of the photons the interference develops primarily in the region of the telescopes used to detect the photons, far away from their source, in the pion interferometry case the interference develops near the source, as soon as the pions undergo their last rescattering and leave the nuclear fireball.

EXPERIMENTAL SETUP

This experiment was performed using the Heavy Ion Spectrometer System [18] (HISS) which is located at the Lawrence Berkeley Laboratory BEVALAC. The HISS facility was designed in a modular fashion to allow one to configure its array of detectors to run a wide variety of experiments.

The core of the HISS facility is the large superconducting dipole magnet. The HISS magnet has pole tips which are 2.1 m in diameter separated by a 1 m gap. It has a maximum central field strength of 3 T, and is mounted on a rotating base.

The HISS configuration used for this experiment is shown in Fig. 1. As the beam from the BEVALAC comes down the evacuated beam line to the HISS experimental cave it impinges onto a soft-collimator (scintillator with hole, put in as veto), monitor scintillator arrangement (V_1 and S_1), also in vacuum, which collimates the beam accepted and sets all the timing in the trigger. The beam continues down the beam pipe, through a dipole and three quadrupole magnets. The beam leaves vacuum and traverses P_1, about 2.5 m of air, and P_2. P_1 and P_2 are position sensitive scintillation detectors which give the upstream vector for the beam. The beam then goes through another soft collimator, scintillator arrangement and enters the vacuum chamber of the HISS superconducting dipole. For this experiment the magnetic field of the HISS dipole was pointing down (into the page) and had a magnitude of 7 kG. The beam then strikes the target located just off center in the HISS magnet. Any surviving beam or projectile fragments then leave the vacuum chamber, strike the trigger detector (V_4), and finally register in the fragment time-of-flight (TOF) wall, following the dotted line in Fig. 1. The negatively charged pions [produced around 0° in the center of mass (c.m.)] and light positively charged particles and nuclei ($\approx$90° in the c.m.) travel through the HISS drift chambers and strike the arc of TOF walls as shown in the figure. The upstream beam vector obtained from P_1 and P_2 and the downstream vectors for the pions obtained from the drift chamber are used to determine the pion's momentum.

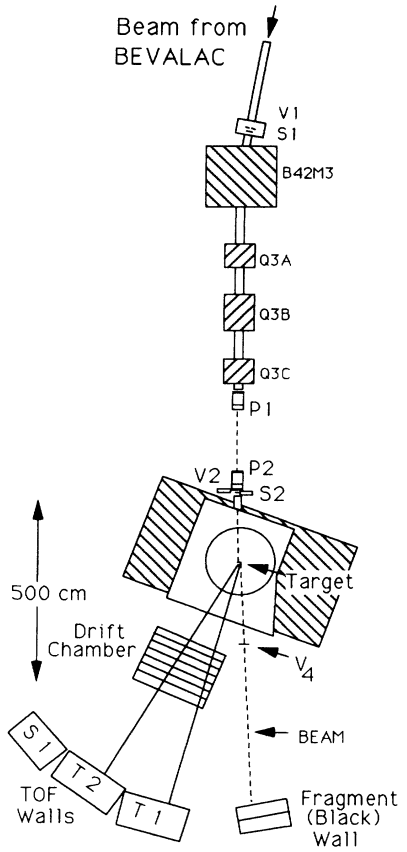

FIG. 1. Experimental setup. HISS B field is into the page with a magnitude of 7 kG.

All of the targets used in this experiment were mounted on a target wheel inside the HISS dipole vacuum chamber.

The trigger detector referred to as V_4 is the one which determined the centrality of the events which the trigger circuit accepted. It consisted of a 50 cm by 30 cm rectangle of 3 mm thick Pilot 425 plastic Cherenkov radiator. We choose to use a Cherenkov radiator to avoid the saturation in the light output which one observes in plastic scintillators for highly charged fragments. The radiator was read out at both ends via adiabatic plastic light pipe by 5 cm photomultiplier tubes. This scintillator was mounted just downstream of the HISS vacuum chamber such that the beam spot was centered on the detector's active area. It was mounted with the long dimension vertical, 235 cm downstream from the center of the HISS dipole.

The TOF covering the fragmentation region consisted of 15 individually wrapped plastic scintillator slats. Each slat is 89.5 cm long, 10 cm wide, and 6 mm thick. The slats are mounted vertically, long edge to long edge, in a plane, on an aluminum frame. On each end of each slat there is attached a tapered plastic light pipe which goes to a 5 cm photomultiplier tube. We collected time and analog information from each end of each slat in the data stream. This TOF wall was incorporated into the experiment to give information on the charge sum of any surviving projectile fragments, and hence give us some

means of estimating the impact parameter. With the gains we used for this wall one may extract the charge of the projectile fragments down to about charge four. Below this point one cannot clearly identify the charge peaks.

The downstream tracking was done using the HISS drift chamber [19] (DC). The overall dimensions of the DC, as seen by a track, are 1.5 m vertically, 2.0 m horizontally, and 1.4 m deep. The detector consists of fifteen modular planes of drift cells. The planes are separated from one another by 10 cm along a line normal to the front plane of the DC, and are all contained in the same gas volume. The planes have one of three types of wire orientation, vertical, and tilted to the left or right of vertical by 30°. The counting gas we used in the DC was P-10 (90% argon, 10% CH_4). The single plane position resolution obtained was ~ 700 μm and the single plane efficiency of the chambers was approximately (within $\approx 1\%$) 100%.

The TOF walls labeled $T1$ and $T2$ consist of twenty slats each. Each slat is 10 cm wide, 300 cm tall, and 2.5 cm thick. There is a plastic, tapered light pipe attached to each end of the slats which is coupled onto 5 cm photomultiplier tubes. From each tube we collect both analog and time information.

The information from the TOF walls allows one to extract the velocity, and hence the mass of the particles for which one gets tracks from the drift chamber. The arc of the TOF walls covered the angles from about 10° to about 55° in the laboratory as shown in Fig. 1.

Targets and beams

We used two targets and two beams in this experiment; they are specified in Tables I and II.

The values listed in Table I for the beam parameters β, γ, K.E., and P are the values at the target after correcting for material upstream in the beam line. The values given for the multiple Coulomb scattering (MCS) (θ_0) are calculated for a pion with a laboratory momentum of 600 MeV/c which traverses half of the target thickness. The effect of this MCS on the overall momentum resolution for the pions is discussed in the section on the momentum reconstruction and resolution. The column labeled L_R gives the radiation lengths of the target materials.

The beam energies used are the maximum available from the BEVALAC for each beam. The target thicknesses were chosen to give a sufficient data rate while keeping the multiple Coulomb scattering and energy loss in the target tolerable.

TABLE II. Target parameters.

Target	Thickness (g/cm^2)	L_R (g/cm^2)	θ_0 (mrad)
KCl	1.130	18.5	4.2
La	0.446	7.8	5.0
Empty			

Triggers

A LeCroy Programmable Logic Unit (PLU) was used for defining the triggers in this experiment. This allows one to switch between a fixed set of triggers, ensuring reproducibility. The targets were cycled run to run to minimize any time-dependent systematics in the data.

The following triggers were used in the experiment.

Beam Straight (BS)$\equiv S_1 \cdot \overline{V_1} \cdot S_2 \cdot \overline{V_2}$. This trigger was what we designated as the Beam trigger. It placed a lower bound on the ADC signals for scintillators S_1 and S_2, and an upper bound for the soft collimators (hole scintillators) V_1 and V_2. The threshold on S_2's discriminator was set at a level just below the signal for the beam, thus eliminating beam tracks which interact in the vacuum window at the end of the beam pipe, P_1 or P_2, or the ≈ 3 m of air upstream of S_2.

Soft$\equiv$BS$\cdot\overline{V_4}$ hi. This trigger is very similar to the trigger used by some members of the collaboration earlier to select central (small impact parameter) events in pion studies using the Streamer Chamber detector at the BEVALAC. As stated explicitly above, the trigger required the BS trigger as well as the lack of a signal from a discriminator connected to V_4. This trigger corresponded to a cutoff in the maximum projectile fragment charge at about $Z = 11$ or 12 for the Ar beam. This trigger was not used for the Xe beam.

Hard$\equiv$BS$\cdot\overline{V_4}$ lo. This trigger was set to select central events. The difference between this trigger and the soft trigger is that the threshold on the discriminator used was set such that the leading fragment charge for the events accepted was something less than ≈ 3 for the Ar beam.

Using the ratio of soft (hard) to BS triggers, corrected for the dead time and the target out ratio, one may calculate the cross section for satisfying the soft (hard) trigger.

In Table III we have summarized the trigger cross sections for the beams and targets used in this analysis.

ANALYSIS

The analysis is performed in four passes through the data. The main task in the first pass through the data is

TABLE I. Parameters of beams used. Note β, γ, K.E., and P are values at target.

Beam	Z	A	β	γ	K.E. (A MeV)	P (GeV/c)
Argon	18	40	0.940 11	2.9336	1799	102.663
Xenon	54	136	0.896 9	2.261	1175	256.726

TABLE III. Summary of triggers. $\sigma_{geo}=\pi r_0^2(A_b^{1/3}+A_t^{1/3})^2$, $r_0=1.2$ fm, and A_b and A_t are the number of nucleons in the beam and target nuclei.

Beam	Target	σ_{geo} (b)	σ_{soft} (b)	$\sigma_{soft}/\sigma_{geo}$ (%)	σ_{hard} (b)	$\sigma_{hard}/\sigma_{geo}$ (%)
Argon	KCl thick	2.116	1.428	67	0.555	26
Argon	La	3.346	2.438	73	1.358	40
Xenon	La	4.856	3.844	80	1.75	37

to construct the tracks in the drift chamber from the wire hits (wires within an event which receive a valid TDC value).

In the second pass through the data the tracks in the drift chamber and the position and angle of the beam on the target, given by P_1 and P_2, are used to reconstruct the π^- momenta.

In the third pass the correlated and uncorrelated pion pairs are formed and placed into matrices. All the systematic corrections to be applied (Gamow, background correlations, DC efficiency, etc.) are calculated and applied to the uncorrelated pairs.

In the fourth pass the multidimensional fitting is performed on the matrices to obtain the best fit to the correlation function and hence extract the spatial (R, or $R_\perp$ and $R_\parallel$), temporal (τ), and "chaoticity" (λ) fit parameters.

Momentum resolution

The momentum resolution for the experimental setup was extracted using a combination of Monte Carlo simulations and information contained in the data. The effects accounted for are MCS in the target, MCS in all material downstream of the target to the back (exit) side of the DC, position and angle resolution of the DC, and the error in the determination of a beam track's position on the target. Figure 2 shows the momentum resolution in the c.m. frame. The squares represent the momentum resolution when all the effects listed above are included. The error in the momentum of the pions due to the position resolution of the beam on the target cancels out to first order in the correlation analysis as one will always be dealing with the relative momentum of the pions. The triangles represent the resolution ($\Delta P/P$) of importance in this analysis which is $\approx 2.5\%$ in the c.m. frame.

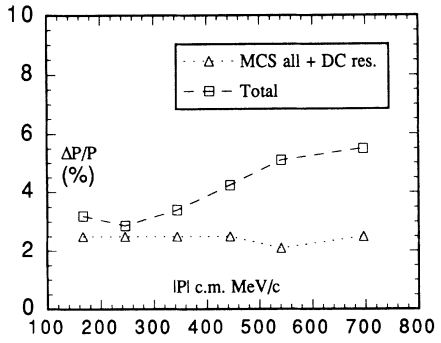

FIG. 2. Momentum resolution evaluated in the nucleon-nucleon c.m. frame. Squares represent π^- momentum resolution due to all effects. Triangles include all effects except position resolution on the target. This (triangles) is the resolution of interest for this analysis.

Particle identification

Using the velocity information from the TOF walls, we observed that the negative particle spectrum contains essentially only π^-'s, as one would expect at these energies as the production cross sections for K^- are about four orders of magnitude smaller [20] than for π^-. Thus, for the negative pion correlation analysis presented here, one need only separate the negatively charged particles from the positively charged particles. One then identifies all of the negatively charged particles as π^-'s. The information we use to distinguish between the positively and negatively charged particles is the position-angle (in the bending plane) correlation of the tracks in the drift chamber. We calculate the contamination of the π^- data due to electrons, resulting from gammas from π^0 decays which convert in the target, to be less than 0.5%.

Systematic corrections

There are five systematic effects which were investigated in the analysis, three of which we have corrected for. In all cases the systematic corrections are applied by weighting the uncorrelated π^- pairs.

The first correction is for the detection efficiency of the DC, due to both hardware and software, in finding close tracks. It is crucial when one does a two- (or multiple-) particle correlation analysis that one understands and characterizes the efficiency of the tracking detectors and software for finding close tracks within an event. As the tracking efficiency is directly dependent on the geometry of the DC cell structure (primarily depends on the vertical wires for the tracking algorithm used), the efficiency curve was parametrized as a function of the spatial separation of the tracks. This is a very small correction used in weighting the background pairs. The effect of this efficiency correction on the HBT fits was very small (see Table IV where we have included the results of the HBT fits with no systematic corrections applied). The multiplicity dependence of the efficiency curve was investigated and found to be negligible over the range of multiplicity observed in the data.

The second correction is for the effect due to the mutual Coulomb repulsion between the pions in the correlated pairs. For the repulsive Coulomb interaction between the two π^- in a pair this penetration factor is the Gamow

TABLE IV. Results for 1.8 A GeV argon on KCl, hard trigger.

Systematic Corrections Applied	DC efficiency Gamow Background		X	X X	X X X
R (fm)		4.46	4.46	4.51±0.14	4.30±0.14
τ (fm/c)		0.0	0.0	0.0+1.1	0.0+1.1
λ		0.56	0.57	0.76±0.05	0.78±0.05
χ^2		753.2	750.3	750.0	745.1
NDF		726	726	726	726
Pr ($\chi^2 \geq \chi^2_{\text{meas}}$)		0.15	0.18	0.18	0.23
89 847 correlated π^- pairs, 1389 400 uncorrelated π^- pairs					
$R_\perp$ (fm)		4.51		4.62±0.18	4.39±0.15
$R_\parallel$ (fm)		3.44		3.63±0.33	3.48±0.30
τ (fm/c)		1.98		$1.08^{+1.12}_{-1.08}$	$1.30^{+0.90}_{-1.30}$
λ		0.55		0.75±0.04	0.77±0.05
χ^2		2107.2		2093.6	2088.3
NDF		2081		2081	2081
Pr ($\chi^2 \geq \chi^2_{\text{meas}}$)		0.28		0.39	0.43
88 709 correlated π^- pairs, 1357 500 uncorrelated π^- pairs.					

factor [11]:

$$G(\eta)=\frac{2\pi\eta}{e^{2\pi\eta}-1}, \quad \text{where } \eta=\frac{m_\pi \alpha}{\sqrt{q_0^2-q^2}} . \tag{7}$$

The Gamow correction factor is applied to the uncorrelated pion pairs before the HBT function is fit. The Gamow correction has a substantial (increases by $\approx 4\sigma$) effect on the λ parameter and a relatively small (increases by $\approx \sigma/3$) effect on the radius parameter (see Table IV). For the argon on KCl, hard trigger data set, the application of the Gamow correction raises the value of λ from 0.57 to 0.76 and raises the value of R from 4.46 to 4.51 fm. The magnitude of the correction on λ is very similar to some earlier results [21].

The third correction is for residual correlations in the uncorrelated pairs. This correction technique was first derived and applied by Zajc [15] in his analysis of a pion interferometry experiment using the Janus spectrometer at the BEVALAC. Its purpose is to correct for the distortion in the single pion inclusive spectra due to the Bose-Einstein correlations. The correction is performed with an iterative procedure in which one weights the uncorrelated pion pairs [15].

For the Ar on KCl, hard trigger data set, this correction lowers the values for the radius parameter R by slightly more than 1σ, from 4.51 down to 4.30 fm. It has no effect on the lifetime parameter τ, leaving it at zero, and increases the λ parameter by about half a σ, from 0.76 to 0.78.

The fourth systematic effect is that due to the finite momentum resolution of the experimental setup. It was seen that the effect of our finite momentum resolution lowered the values of the HBT fit parameters by less than 2%, which corresponds to about one-half of the standard deviation for the most precise fit. Due to the small magnitude of this correction, and the approximate method in which it is calculated [13], we note it for completeness but it has not been applied to any of the results presented here.

The final systematic effect that we include here for completeness is the Coulomb attraction between any remaining projectile spectator fragment and the negatively charged pions. These effects have been seen in inclusive pion studies [22] as an enhancement of the ratio of the π^- to π^+ cross sections for momenta close to that of the projectile. In previous experiments [15,23–25] attempts have been made either to correct for this effect or to cut out the data thought to be affected. To correct for this effect one must either know, on an event by event basis, the mass, charge, and momenta of the projectile fragments, or one must choose what one believes to be a reasonable distribution for these quantities. One then corrects, on a component by component basis, the momentum of the pions. The other method is to transform all the pion momenta into the projectile frame and then place a threshold on the pion momenta in this frame.

We investigated the effect of this Coulomb attraction, employing both of the techniques above, and concluded this effect is negligible for this experiment. As the upper limit of the effect is less than the uncertainty obtained in fitting the data, and depends either on one's choice for the projectile fragments and their momenta, or on one's assumptions about the charge, size, and temperature of the fireball, we do not apply this correction in the final fits to the data. The size of the effect calculated is very similar to that which others have found [15,25] doing this type of analysis.

Phase Space acceptance

Figures 3, 4, and 5 show the acceptance of the experimental setup due to constraints of both the hardware and

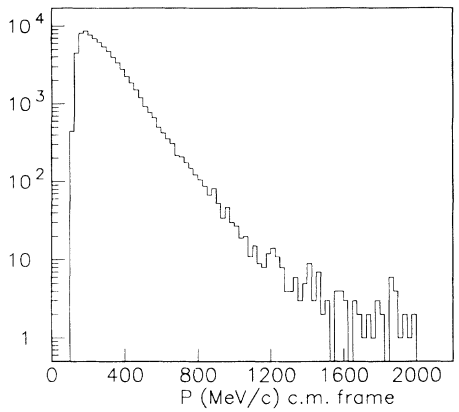

FIG. 3. Inclusive momentum distribution for the π^-, evaluated in the nucleon-nucleon c.m. frame, for events with 2 or more π^-.

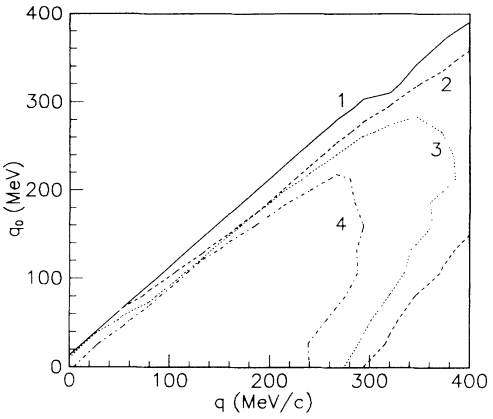

FIG. 5. Acceptance for correlated π^- pairs. q and q_0 are the relative momentum and energy, respectively, for the pairs. Increasing contour labels represent increasing numbers of counts.

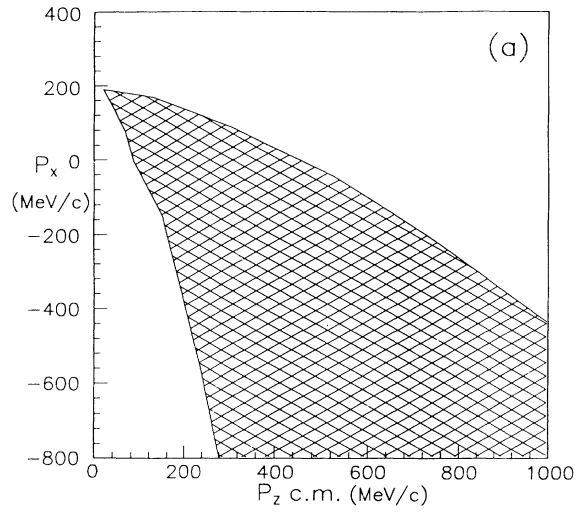

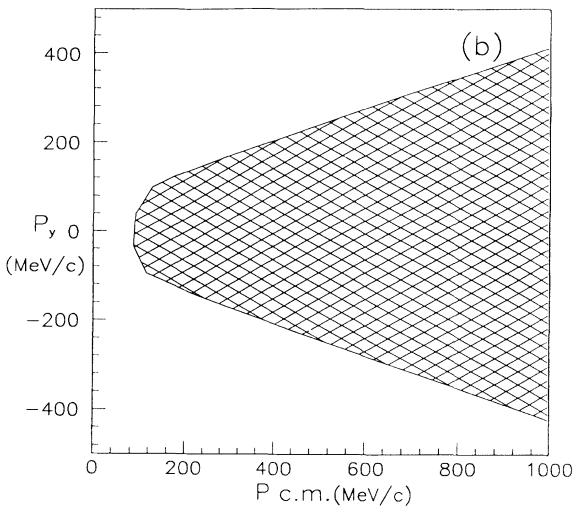

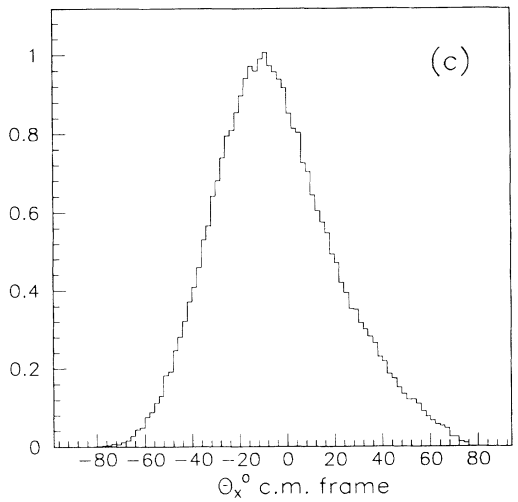

FIG. 4. Crosshatched regions in (a) and (b) show the acceptance for π^- in Ar on KCl data set. X is in bending plane of HISS dipole, Y is vertical, and Z is along beam direction. The inclusive θ_x distribution shown in (c) has a mean of 5° and $\sigma \approx 25°$.

the analysis software. All the plots shown in this section are from the Ar on KCl, hard trigger data set. The coordinates are defined such that P_x is the component of momentum in the bending plane of the HISS dipole, P_y is the vertical or out of bending plane component, and P_z is the component in the direction of the beam, i.e., longitudinal component.

Figure 3 shows a histogram of the inclusive momentum distribution for the negative pions in the nucleon-nucleon c.m. frame which are accepted into the HBT analysis (i.e., come from events with two or more π^-). Figure 4(a) shows the acceptance in P_x vs P_z, evaluated in the nucleon-nucleon c.m. frame. Figure 4(b) shows the acceptance in P_y versus the magnitude of the momentum, evaluated in the c.m. frame. Figure 4(c) shows the inclusive distribution of θ_x in the c.m. frame for a random subset of the pions used in the correlation analysis. They come from a distribution of angles with a mean of about $-5°$ and a σ of about 25°.

Figure 5 shows the acceptance for the pion pairs, in particular the distribution for the relative momentum of the pairs (q) and the relative energy of the pion pairs (q_0). The increasing contour labels represent increasing numbers of counts. Notice that only half of the q-q_0 plane is populated. This is due to a constraint imposed by relativistic kinematics.

RESULTS

The results are subdivided for the various beam-target-trigger combinations. In each subsection we have tabulated the fits to the two forms of the correlation function given below:

$$C_2(q,q_0)=N(1+\lambda e^{(-q^2R^2/2-q_0^2\tau^2/2)}) \tag{8}$$

and

$$C_2(q_\perp,q_\parallel,q_0)=N(1+\lambda e^{(-q_\perp^2R_\perp^2/2-q_\parallel^2R_\parallel^2/2-q_0^2\tau^2/2)}) . \tag{9}$$

The parameter N is merely a normalization factor and is of no physical significance. All the fits for the symmetric beam-target systems were performed in the nucleon-nucleon center-of-mass system.

The results of the fits are shown with the following combinations of systematic corrections applied: no corrections, both the DC efficiency and the Gamow corrections, and the DC efficiency, Gamow, and correction for Background correlations all applied. For the argon on KCl hard trigger data, the results are also shown with only the DC efficiency correction applied to illustrate how small this correction is. Where calculated, the one σ errors in the fit are given for the parameters. Also listed in the tables are the χ^2 and the number of independent degrees of freedom (NDF) for the fit. Using these two quantities we have calculated what is known [26] as the *Upper-tail area function* using the first approximation to χ^2. This Upper-tail area function (UTAF) gives the probability of getting a value for χ^2 greater (or less) than that measured. Its value is the percentage of the area of the χ^2 distribution between the value for χ^2 which one obtains from the fit to the nearest end of the distribution. For a perfect fit this function reaches its maximum value of one-half. For all fits the range of the independent variables (i.e., q, q_0,$q_\perp$,$q_\parallel$) was from 0 to 400 (MeV/c, MeV).

The tables given in the subsections also contain the number of correlated and uncorrelated π^- pairs used in each of the fits. The variation in the number of π^- pairs used in the various fits for a given beam-target-trigger combination is due to the different numbers of matrix bins used into which the pairs are placed [i.e., $C(q,q_0)$ or $C(q_\perp,q_\parallel,q_0)$] and the requirement that all bins used in the fits contain at least five correlated pairs.

Hard trigger data

Argon on KCl

The trigger selected $\approx$26% of the geometric cross section for the argon on KCl system. Approximately 6.5% of the events accepted by the trigger contained two π^- which were passed for further analysis. We collected approximately 1.2 to 1.5 million raw events and ended up with $\approx$90 000 correlated pion pairs which passed all the cuts and acceptance limits. Bin widths of 10 MeV (MeV/c) were used in the first set of fits in the table and widths of 20 were used in the second set of fits [$C_2(q_\perp,q_\parallel,q_0)$]. The results are listed in Table IV.

Figure 6 shows the experimental correlation data (i.e., the distribution as a function of q and q_0 of the correlated π^- pairs divided by the same distribution for the uncorrelated pairs) in Fig. 6(a) and the fitted theoretical correlation function in Fig. 6(b). The data and fit shown correspond to the first set of fit parameters in Table IV, with the DC efficiency and Gamow corrections applied. Notice the expected enhancement in the ratio of correlated to uncorrelated π^- pairs in the low q-q_0 region. Bin widths shown are 10 MeV/c by 10 MeV.

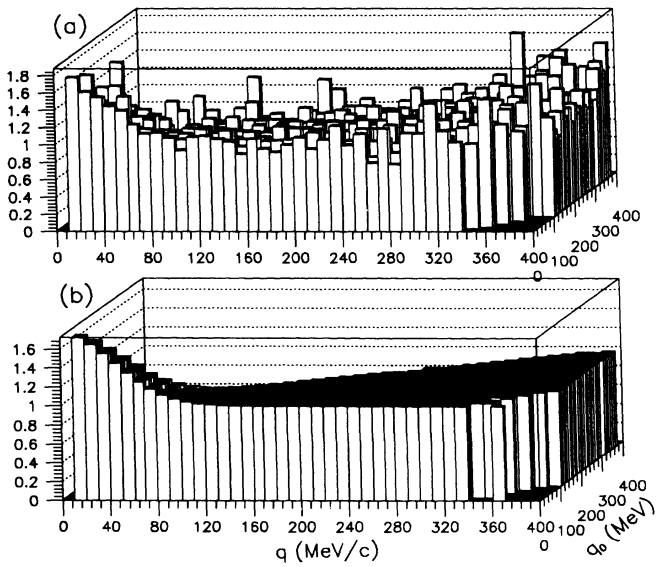

FIG. 6. $C(q,q_0)$ vs q and q_0 for Ar on KCl, hard trigger data set. (a) The experimental correlation data and (b) the fit. The DC efficiency and Gamow corrections are applied.

As the extracted lifetime parameter is zero for the data and fit shown, and because historically others have shown correlation results in this manner, Figs. 7(a) and 7(b) show the same set of data and the fit, without and with the DC efficiency and Gamow corrections applied, projected onto the q axis. The error bars shown are just the statistical errors. The dashed lines are the fitted HBT function.

When one plots the error contours, the correlation between the various fit parameters can be examined. Shown in Fig. 8 are the error contours for the same data as shown in Fig. 7(b), where the DC efficiency and Gamow corrections are applied. The contours shown correspond to the one and two standard deviation errors. The positive correlation shown between the chaoticity parameter λ and the radius parameter R is as one would expect: an increase in R can be compensated for by an increase in λ, and has been seen by others. The lack of any correlation between the radius and lifetime parameters (i.e., error contours are parallel to the axes) is a consequence of the large acceptance of the experimental setup, which has the desirable effect of uncoupling the determination of the two parameters.

Figure 9 shows the error contours for the spatial parameters $R_\perp$ and $R_\parallel$ versus those for the lifetime parameter τ. Notice the correlation between the parameters $R_\parallel$ and τ and the lack of a correlation between the parameters $R_\perp$ and τ. This is to be expected due to the coupling of the relative energy and the relative parallel momentum

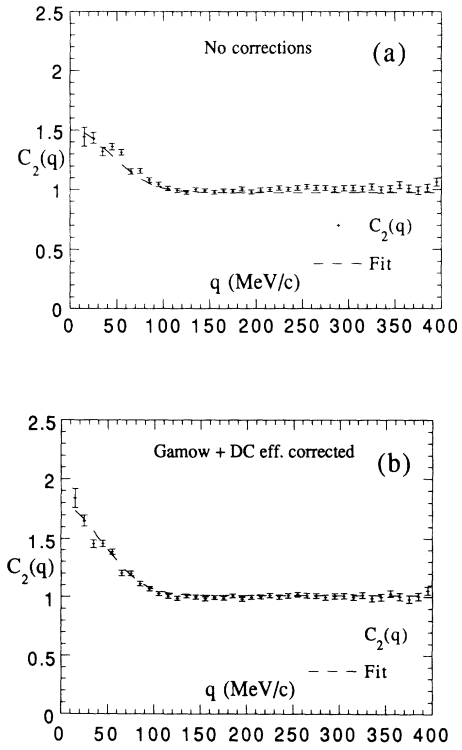

FIG. 7. The correlation function projected onto the q axis for the data shown in Fig. 6. Uncertainties shown are statistical. Notice the clear enhancement of the correlation region even in the raw data.

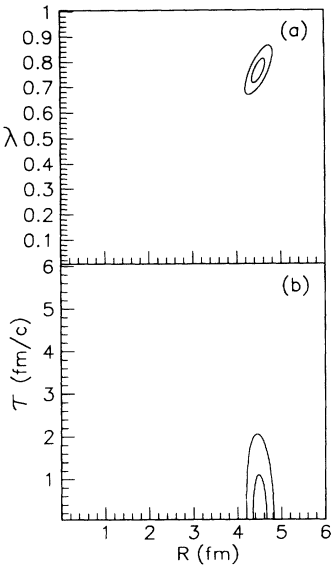

FIG. 8. 1σ and 2σ error contours for standard R,τ,λ fit. Data are Ar on KCl, with the hard trigger. DC efficiency and Gamow corrections are applied.

for pions observed near zero degrees.

It has been suggested by Beavis *et al.* [27] and by Pratt [28] that one may be able to extract information about the evolution of the pion emitting source by performing the HBT analysis as a function of the mean momentum of the pion pairs in the c.m. frame. Pratt's model incorporates the radial expansion aspects of the hot participant region, as theorized by Siemens and Rasmussen [29], to see how the pion interferometry analysis is affected. What he finds is that the radius parameter R decreases monotonically as a function of K ($K=p_1+p_2$), and that

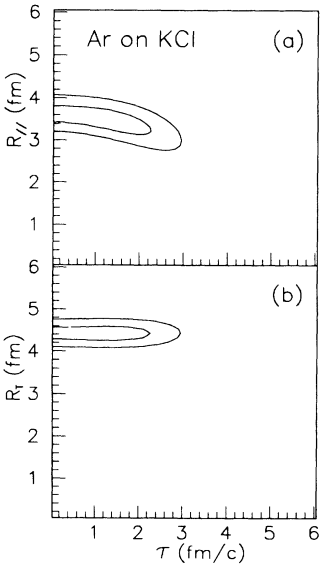

FIG. 9. 1σ and 2σ error contours for $R_\parallel$ vs τ and $R_\perp$ vs τ. Ar on KCl, hard trigger data set. Notice the coupling between the parameters $R_\parallel$ and τ and the absence of any coupling (error contours parallel to axes) between $R_\perp$ and τ. DC efficiency, Gamow, and background correlation corrections are applied.

R decreases faster as the ratio of the energy in collective expansion to thermal energy is increased. The physical explanation Pratt gives for this effect is that the faster pion pairs are most likely emitted from a point on the expanding shell which is in the direction of K, and therefore appear to come from a smaller effective source. He also points out that another possible explanation could be that as the pion-nucleon cross section falls off rapidly for relative energies above 140 MeV due to the delta resonance, the fast pions may have a larger mean free path and hence a higher probability of escaping during the early stages of the collision while the source is small.

In Fig. 10 we show the results obtained when we binned the pion pairs as a function of their mean summed momentum in the nucleus-nucleus c.m. frame. The requirement imposed to determine the binning was that one get equal numbers of correlated π^- pairs with relative momentum (q) less than or equal to 50 MeV/c in each bin. We imposed this requirement in an attempt to get roughly equal sensitivity for the various HBT fit parameters in all the bins. The vertical error bars correspond to the one sigma errors in the HBT fits. The horizontal error bars correspond to the standard deviation for the distribution of the mean pion pair momentum within the bin. The fits shown have the drift chamber efficiency and Gamow corrections applied.

The plots shown in Fig. 10 are suggestive of the trend which Pratt predicts. If one believes that this effect is manifesting itself in the plots, it appears that to investigate the effect one should design an experiment which has as low a cutoff in acceptance for pion momentum as possible. It is also clear that one needs very good statistics to pursue this type of study.

The apparent decrease in radius at a mean pion momentum of ≈ 150 MeV/c is very similar to results obtained for 1.5A GeV Ar on KCl data taken at the LBL streamer chamber by Beavis *et al.* [27]. The magnitude of the effect we see is smaller than observed in their data, although one must note that the range of the mean pion momentum in our data is also smaller. As pointed out in their paper, the decrease of the extracted radius as a function of the pion momentum is consistent with a pion fireball model in which the temperature decrease as the source expands. In a later paper by the same group for 1.8A GeV Ar on Pb this effect of a decreasing radius as one increases the mean value of the pion pair's momentum was also observed [25].

Shown in Fig. 11 are the unnormalized inclusive π^- cross sections versus the kinetic energy of the pions in the c.m. frame, for three angles in the c.m. frame. The data are from the 1.8A GeV argon on KCl, hard trigger data set. The cross sections shown have not been corrected with target out data. The error bars shown are just those due to statistics. The main feature to notice in this plot is the characteristic exponential falloff in the cross section as a function of the pions kinetic energy.

For a slightly more quantitative evaluation of the inclusive π^- cross sections we have fitted a subset of the 22° cross sections to the following equation:

$$E\frac{d^3\sigma}{dp^3}=ce^{(-\mathrm{K.E.}_{\mathrm{c.m.}}/E_0)} . \tag{10}$$

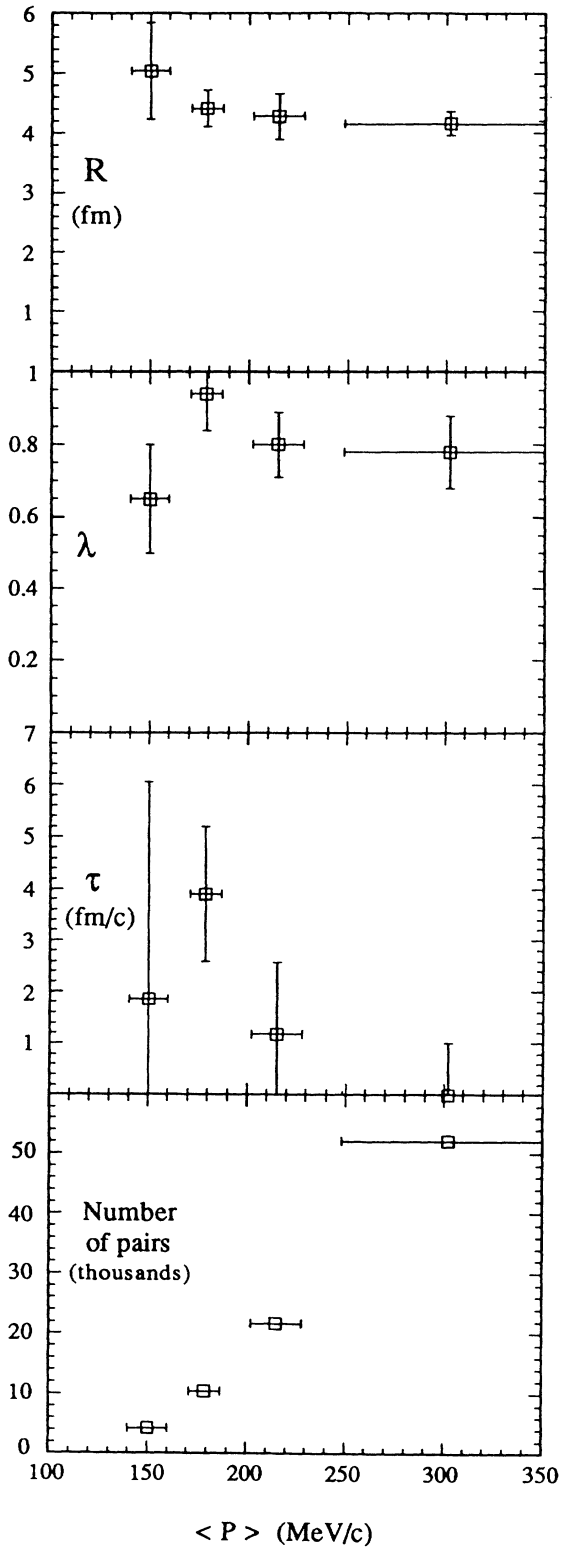

FIG. 10. Standard R,τ,λ fit parameters as a function of the mean momentum of the pion pairs in the c.m. frame. Ar on KCl, hard trigger data set. Vertical bars are the 1σ errors from the fit. Horizontal bars correspond to the standard deviation for the pion pair momentum within the bin. Fits shown have dc efficiency and Gamow corrections applied.

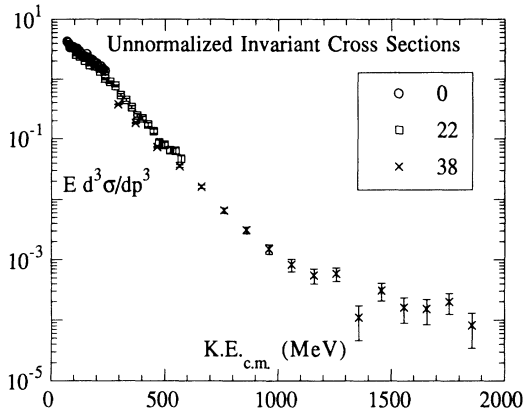

FIG. 11. Unnormalized, invariant, inclusive π^- cross sections versus kinetic energy in the nucleon-nucleon c.m. frame for three angles. Data are Ar on KCl with the hard trigger. Errors shown are statistical.

Figure 12 shows the fit line and the value extracted for what is commonly referred to as the slope parameter, E_0. Shor *et al.* [20] measured this slope parameter for π^- at 0° in the c.m. frame for 2.0A GeV ^{28}Si on ^{28}Si, over a similar range of pion kinetic energy, and obtained the value $E_0=108\pm7$ MeV. Nagamiya *et al.* [30] measured the slope parameter for π^-s at 90° in the c.m. frame from 2.1A GeV Ne on NaF. They obtained the value $E_0=102$ MeV. The only point we wish to make with the above plots, and the slope parameter measurement is the qualitative agreement between the inclusive invariant cross sections measured by others and those from our data set.

Argon on lanthanum

The data presented in this section were taken using the hard trigger. The cross section for satisfying this trigger, for this system, corresponds to ≈40% of the geometric cross section. We collected a total of around 320 000 raw events. Out of these we ended up with about 12 000 to 13 000 correlated pion pairs (depending on whether 10 or 20 MeV bins were used in the fit) and approximately 190 000 uncorrelated pairs, which made it past all the cuts and into the fitting routine.

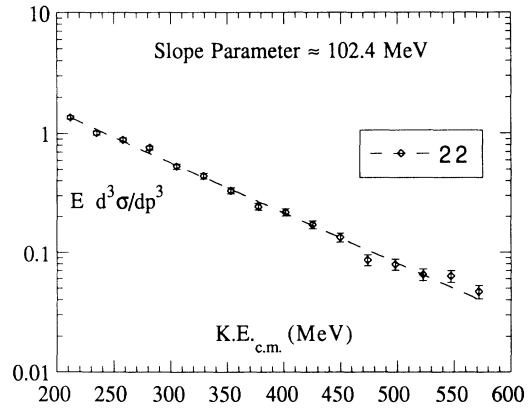

FIG. 12. Fit to the 22° π^- inclusive cross sections from Fig. 11. The fitted slope parameter agrees quite well with those seen by others.

There is an additional complication that comes into question for asymmetric colliding systems such as the argon on lanthanum presented in this section. For symmetric systems one knows that independent of the impact parameter, the interaction region, which is the source for the pions, will reside in the nucleon-nucleon center of mass (c.m.), and thus this is the natural reference frame in which to perform the HBT analysis. For asymmetric systems it is not so obvious in which frame to perform the analysis.

Beavis *et al.* [25] have shown, using the Streamer Chamber at the BEVALAC, that for 1.8A GeV argon on lead, the velocity for the pion source ranges from the *n-n* c.m. frame for the lowest pion multiplicity events, to the minimum c.m. velocity expected (using a geometric model prediction for the number of target nucleons involved) for the highest pion multiplicity events.

Using the clean-cut geometric model for the collision, one may calculate the number of nucleons sheared off of the projectile and target nuclei as a function of the impact parameter. With this information one may then calculate the center-of-mass velocity of the overlap region (assuming full stopping in the c.m.), which is the frame in which the HBT analysis is to be performed, (i.e., the supposed rest frame of the pion source to be measured). We calculated this overlap region velocity for impact parameters of 0 ($\beta_{\text{c.m.}}=0.5588$) and 2.1 fm ($\beta_{\text{c.m.}}=0.5704$). The 2.1 fm case corresponds to the maximum impact parameter such that the argon nucleus is completely occluded by the lanthanum nucleus.

To see what effect this choice of frame has on the HBT analysis we transformed all the pions into the two frames and performed the fits. In both frames the lifetime parameter came out to zero. Within the reasonable range of rest frames for this experiment, the variations in the parameters R and λ were all within one σ of one another.

One expects the combination of our central collision trigger, and the requirement that all events in the analysis have at least two π^- within the spectrometer's acceptance, to heavily bias the events toward those with a small impact parameter. On this basis we believe that the true average rest frame for the pion source is probably in the range of $0.5588\leq\beta_{\text{c.m.}}<0.6$. As the dependence of the fit parameters on the choice of frame is small (relative to the uncertainties) in this region, and a choice must be made, all fits for the Ar on La are performed in the frame with $\beta_{\text{c.m.}}$ equal to 0.5704 ($b\approx2.1$ fm). The results are listed in Table V.

Xenon on lanthanum

The results for a 1.2A GeV xenon beam incident on a lanthanum target are listed in Table VI. This set of data was taken using the hard trigger. The cross section for satisfying this trigger, for this system, corresponds to ≈37% of the geometric cross section. A total of ≈320 000 raw events were collected for this configuration, out of which we ended up with about

TABLE V. Results for 1.8A GeV argon on La, hard trigger.

Systematic Corrections Applied	None Gamow+DC_{eff} Background	X	X	X / X
R (fm)		4.01	4.11±0.28	3.88±0.28
τ (fm/c)		0.0	0.0±1.0	0.0±1.0
λ		0.80	1.02±0.12	1.05±0.13
χ^2 / NDF		186.2 / 178	191.0 / 178	193.3 / 178
UTAF		0.26	0.16	0.12
12 293 correlated π^- pairs, 191 640 uncorrelated π^- pairs				
$R_\perp$ (fm)		4.60	4.82±0.45	4.63±0.40
$R_\parallel$ (fm)		3.88	3.80±0.53	3.82±0.50
τ (fm/c)		0.0	0.0±1.90	0.0±2.0
λ		0.82	1.06±0.13	1.10±0.14
χ^2 / NDF		564.0 / 548	562.3 / 548	559.5 / 548
UTAF		0.24	0.26	0.30
9485 correlated π^- pairs, 138 710 uncorrelated π^- pairs				

10 000 correlated π^- pairs which passed all the cuts and made it into the HBT analysis.

There are a few points to notice in Table VI. The first is the rather large (relative to the previous data sets) value for the lifetime parameter τ in the standard R,τ,λ fit. As is the case with every fit performed in this experiment, however, due to the large error on τ it is still consistent with zero. In the second set of fits presented in the table one sees that, given the freedom, the fits return a large value for the parallel radius and again return lifetime parameters of zero. This is another illustration of the coupling between q_0 and $q_\parallel$, and hence the fit parameters τ and $R_\parallel$, one expects for interferometry studies centered on zero degrees. Whereas the fit source shapes for both the Ar on KCl and the Ar on La were oblate, the Xe on La results above indicate a prolate ($R_\parallel > R_\perp$) pion source.

Soft trigger data

This section contains the results for the Ar on KCl data taken with the soft trigger. The cross section for satisfying this trigger, for this system, corresponds to ≈67% of the geometric cross section.

Our goal with this trigger was to see if we could show a direct correlation between the impact parameter of the

TABLE VI. Results for 1.2A GeV xenon on La, hard trigger.

Systematic Corrections Applied	None Gamow+DC_{eff} Background	X	X	X / X
R (fm)		5.15	5.40±0.8	4.90±0.75
τ (fm/c)		4.60	$3.60^{+2.2}_{3.6}$	$3.44^{+1.9}_{3.4}$
λ		0.53	0.80±0.19	0.76±0.17
χ^2 / NDF		218.1 / 158	218.1 / 158	220.25 / 158
UTAF		5×10^{-6}	5×10^{-6}	2×10^{-6}
10 241 correlated π^- pairs, 162 280 uncorrelated π^- pairs				
$R_\perp$ (fm)		5.11	5.56±0.63	5.40±0.65
$R_\parallel$ (fm)		8.75	7.94±1.5	7.70±1.40
τ (fm/c)		0.0	0.0+3.60	0.0+3.60
λ		0.60	0.90±0.18	0.91±0.18
χ^2 / NDF		455.8 / 394	451.8 / 394	450.0 / 394
UTAF		1.2×10^{-3}	2.3×10^{-3}	3.0×10^{-3}
8155 uncorrelated π^- pairs, 123 720 uncorrelated π^- pairs				

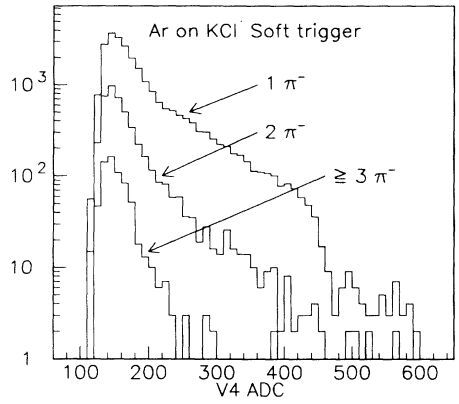

FIG. 13. Histograms of the ADC (proportional to the projectile fragment charge) for the Cherenkov radiator (V_4) with software requirements of 1, 2, and ≥ 3 π^- observed within our acceptance. Ar on KCl, soft trigger data. Notice the expected biasing toward central collisions as one requires 2 or more π^-.

collision, as deduced from the charge of the leading projectile fragment, and the extracted HBT radius parameter. We collected a total of $\approx 500\,000$ raw events with this trigger, out of which we ended up with $\approx 17\,400$ correlated π^- pairs.

As one would expect with a trigger of this sort, when one imposes the software requirement that an event must have two negative pions within our experimental acceptance there is a heavy biasing toward central events. This effect can be seen in Fig. 13 which shows a histogram of the signal in the Cherenkov (V_4) radiator used in the trigger for various cuts on the number of π^- observed.

The table of results for this beam-target-trigger combination is organized a little differently than the previous three sections. We again show the results of fits to the two forms of the correlation function, but the results are also given for three different requirements on the maximum fragment charge observed in the fragment TOF wall (placed to detect projectile fragments, see Fig. 1). The criterion used to determine the placement of this cut was that there be approximately equal numbers of correlated π^- pairs above and below the cut.

For the results shown in Table VII, bin widths of 10 MeV/c (MeV) were used in the first set of fits (R,τ,λ) and widths of 20 MeV/c (MeV) were used in the second sets of fits. The dc efficiency and Gamow corrections are applied in all the fits shown. The background correlation correction is not applied.

The results shown in Table VII exhibit the trends which one would expect. The fit value for the standard radius parameter R is largest for the cut selecting the lower portion of the fragment wall charge spectrum, smallest for the high cut, and in between the high and low when no cut is made. This behavior is also shown in the perpendicular ($R_\perp$) and parallel ($R_\parallel$) radius parameters, although for the parallel radius parameter in particular the uncertainties are large.

While we cannot make a definitive statement based on these soft trigger data that we see a correlation between the size of the leading fragment ($\propto$ impact parameter) and the extracted radius of the pion source, the trends in the results are suggestive that this correlation exists. We believe that a data set of this type could answer this question if one either acquired a very large data sample with a similar trigger, or devised a trigger which contained a two-pion requirement in addition to a selection on the leading fragment charge.

DISCUSSION

Up to this point we have shown that there is an enhancement in the two-pion cross section for pions which are close to one another in phase space. We have also shown that if one makes the assumption that the pion emitting sources are Gaussian in space and time (the time part to a lesser degree as this analysis technique is

TABLE VII. Results for 1.8 A GeV argon on KCl, soft trigger.

Part of fragment wall ADC distribution	All	Low	High
R (fm)	4.55±0.35	4.83±0.48	4.30±0.48
τ (fm/c)	0+2.0	0+2.8	0+2.8
λ	0.68±0.1	0.70±0.15	0.65±0.14
$\frac{\chi^2}{\text{NDF}}$	$\frac{590.4}{606}$	$\frac{535.6}{479}$	$\frac{382.5}{428}$
UTAF	0.27	0.005	0.012
Number of correlated π^- pairs	17 428	8822	7484
$R_\perp$ (fm)	5.01±0.45	5.72±0.7	4.75±0.50
$R_\parallel$ (fm)	$2.12^{+1.08}_{-2.12}$	$0.90^{+3.10}_{-0.90}$	$2.41^{+0.8}_{-1.2}$
τ (fm/c)	$3.93^{+1.47}_{-1.93}$	$4.33^{+1.1}_{-4.33}$	0+2.40
λ	$0.71^{+0.10}_{-0.06}$	$0.80^{+0.20}_{-0.14}$	$0.58^{+0.14}_{-0.10}$
$\frac{\chi^2}{\text{NDF}}$	$\frac{833.76}{713}$	$\frac{516.6}{431}$	$\frac{391.4}{366}$
UTAF	6×10^{-6}	4×10^{-5}	0.09
Number of correlated π^- pairs	14 646	6721	5730

not very sensitive to the lifetime parameter) we get a good fit to the shape of the theoretical correlation function, and for this data set we can extract fairly precise values for the HBT fit parameters. We present here some simple geometric arguments for the size of the system which set the scale that one would expect.

For the spatial parameter, R, the natural quantities with which to compare are the geometric size of the projectile nucleus and of the interaction region (IR) in the nucleus-nucleus collision. We have tabulated the calculated sharp sphere rms radii (SSRR) for each projectile and for two bounds on the number of participant nucleons, the fit radii converted to equivalent SSRR, and the ratios of the calculated to fit volumes, in Table VIII.

To convert the fit radii to the equivalent SSRR, one multiplies the values in the results tables by the factor 1.52 (see Appendix). The lower bound on the number of participant nucleons is calculated via the abrasion portion of the abrasion-ablation model by equating the abrasion cross section with that of the hardware trigger for each system (i.e., 0.555 b for the Ar on KCl data). This is surely an underestimate for the number of participants as only a small fraction of the events accepted by the trigger contain two or more pions and one expects a biasing toward central events. The upper bound on the number of participants is clearly just the sum of the nucleons in the system for the symmetric case (i.e., 80 for Ar on KCl) and approximately 116 for the Ar on La system (see discussion in Ar on La results section). The errors shown on the ratio are those due the errors in the fit values of $R_\perp$ and $R_\parallel$.

One observation that is generally true for all the experimental results using two-particle interferometry to measure source sizes in relativistic heavy-ion collisions is that the radii one measures are usually greater than the radii of the colliding system. The explanation for this observation is that the correlations which one measures in the relative momentum and energy of the particles, in this case pions, are those that exist after the last rescattering of the particles as they escape from the interaction region. The density which one calculates using the measured HBT spatial parameters and a measured or assumed number of nucleons participating in the collision is thus commonly referred to as the *freeze-out* density for the particular particle used for the interferometry analysis (equivalent to last column in Table VIII). Due to the large π-N scattering cross section pion interferometry is expected to yield information on the later, cooler stages of an expanding system.

With the errors as shown, and the assumptions made for the number of participant nucleons, there does not appear to be any dependence of the freeze-out density on the size of the colliding system. This is consistent with what one would expect from the simple rescattering argument. If it is indeed true that the freeze-out density measured via the HBT analysis is independent of the mass of the colliding system, one could argue that the HBT technique measures the size of the systems at the same point in the evolution of the participant regions of the collisions. This would support the interpretation of the spatial HBT parameters as actually being a useful measure somehow proportional to the spatial distribution of the pion source.

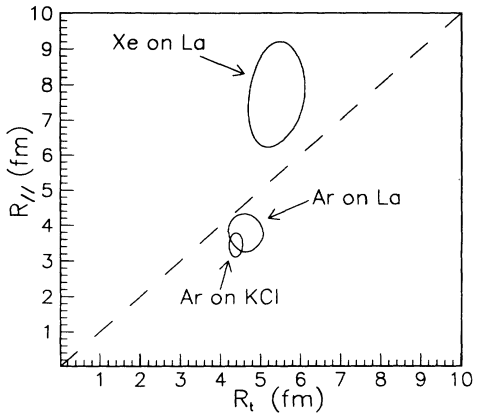

FIG. 14. Summary plot of $R_\perp$ vs $R_\parallel$ for three systems studied. 1σ error contours are shown. Dashed line is for reference and represents $R_\perp = R_\parallel$. DC efficiency, Gamow, and background correlation corrections are applied for all three fits shown.

None of the source shapes measured in this experiment is spherical (within one sigma), although the argon on lanthanum source is very close. In Fig. 14 we show the perpendicular and parallel radii for the three central collision data sets. What is shown on the plot are the one σ error contours for the three system. The dashed 45° line is for reference purposes and corresponds to $R_\perp$ equal to $R_\parallel$. The first feature to note is that the errors in $R_\perp$ and $R_\parallel$ are essentially uncorrelated, as the axes of the error contours are parallel to the coordinate axes. The next feature to notice is that the uncertainty in $R_\parallel$ is larger than the uncertainty in $R_\perp$. This is as one would expect for a study at zero degrees in the c.m. frame due to the coupling between $R_\parallel$ and τ. The next feature to note is the very slight dependence of the perpendicular radii on the size of the colliding system. For the Ar on KCl and

TABLE VIII. Calculated freeze-out densities. The lower bound on the number of participant nucleons (A_{IR}) is derived by equating the abrasion and trigger cross sections. The upper bound for the symmetric systems are the sum of the nucleons in the beam and target nuclei. For Ar on La the upper bound is the number of participants when the Ar nucleus is just occluded by the La nucleus.

Data set	R_{beam} $1.2A_{beam}^{1/3}$ (fm)	A_{IR} (Assumed) Lower	Upper	R_{IR} (fm) $1.2A_{IR}^{1/3}$ Lower	Upper	$R_{meas.}$ (fm) $1.52R_{Fit}$ $\perp$	$\parallel$	ρ_0 (% of NND) Lower	Upper
Ar on KCl	4.10	30–80		3.72–5.17		6.67	5.29	22±3–	59±7
Ar on La	4.10	42–116		4.17–5.85		7.04	5.81	25±5–	70±15
Xe on La	6.11	70–271		4.95–7.76		8.21	11.70	15±5–	59±18

Ar on La data this could be interpreted as an indication that the size of the projectile is the determining factor for the size of the pion source as determined via HBT analyses. Finally, notice that whereas the source shapes for the Ar on KCl and Ar on La are oblate in the c.m. frame, the source shape as measured for the Xe on La system is prolate. We do not know of any arguments that would explain this effect. To investigate this effect further, we recently ran a follow-up experiment using the HISS facility to get a more precise measurement using $1.2A$ GeV ^{139}La on La. Preliminary analysis indicates the source shape is oblate.

The main feature which shows up in the data for the lifetime parameter τ, for all the fits, is that the fit is very insensitive to τ. The insensitivity of the fit to the value of τ is consistent with what Yano and Koonin [10] predicted in their theoretical formulation. This insensitivity is clearly seen by looking at the errors given for τ in the results tables.

Another prevailing feature of the lifetime parameter is that in all cases presented here the errors were such that if the fit value of τ was not identically equal to zero, the errors on the parameter were such that within one σ all the measured values of τ were consistent with zero. The parameter which showed the largest coupling to τ was the parallel radius. This coupling between the parallel radius, which is a function of the relative parallel momentum, $q_{\parallel}$, and τ, which is a function of the relative energy of the π^- pairs, is to be expected in pion interferometry at angles close to 0° in the c.m. system, due to the tight correlation between parallel momentum and energy. This is illustrated graphically in Fig. 9 for the Ar on KCl data set, and can also be seen by looking at the results table for the Xe on La data set.

The usual interpretation of the lifetime parameter is that it is a measure of the time over which the pions are emitted. If one was to apply this interpretation to the results presented here one would conclude that the pions all escape from the pion source instantaneously. This is not the conclusion we draw from the results. We merely conclude that as predicted this type of analysis is insensitive to the lifetime parameter.

This brings us to the chaoticity parameter λ. The historical interpretation of this parameter has been that it allows for a decrease in the magnitude of the two-pion enhancement due to partial coherence of the emitted pions as well as other correlations imposed on the pions. Assuming that one has correctly accounted and corrected for all kinematic and dynamic correlations in the single- and double-pion distributions, it has been theorized that the subsequent value of the chaoticity parameter may give a measure of the degree of coherence of the pion source [11].

If one uses the value obtained for λ in the fits to the central Ar on KCl data ($\lambda \approx 0.75$), and solves for the ratio of coherent to chaotic pions using the formalism of Ref. [11], one ends up with the result that the number of chaotic and coherent pions are approximately equal. As the value for λ obtained from the fit to the asymmetric Ar on La data is approximately equal to one, the calculation would say that all the pions in this data set are from a chaotic source.

One of the same authors referenced for the arguments given above, in a subsequent paper [17], emphasized that unless one has an exclusive data set, and hence can eliminate the averaging over unobserved final states inherent in inclusive measurements, any interpretation one makes of the λ parameter will be suspect at best. One of the examples given of these "ensemble correlations" is the shadowing of the pions, as a function of their angle of emission in the reaction plane of the collision, due to any target or projectile spectator matter.

Another reason that one should be careful in interpreting the λ parameter as having physical significance is the large effect which the Gamow correction has on λ, and therefore the faith that one must put in this correction.

In the data set and fits presented here, the only comment we would like to make on this parameter is that for both the symmetric data sets (Ar on KCl and Xe on La) the values of this parameter are about equal and less than one, whereas for the asymmetric data set (Ar on La) the value is about equal to one.

Comparison with results of others

Comparison of the results obtained here with other pion interferometry experiments is facilitated by the compilation of results in this field published by Bartke [31]. To make a comparison of the extracted radii meaningful, Bartke has tabulated all the necessary conversion factors which one must apply, depending on the experimenter's choice of the theoretical framework to follow and the source distribution to use. All of the radius values plotted have been converted to the root-mean-square (rms) values.

For the results presented here the appropriate conversion factor is $\sqrt{3/2}$ (i.e., multiply values from the results tables given earlier by $\sqrt{3/2}$. This conversion factor is discussed in the Appendix). In Fig. 15 we have plotted the values from Bartke's compilation in essentially the same format as he used and included some recent results of Chacon *et al.* [23,24] as well as the results reported here. The dashed line shown on the plot corresponds to

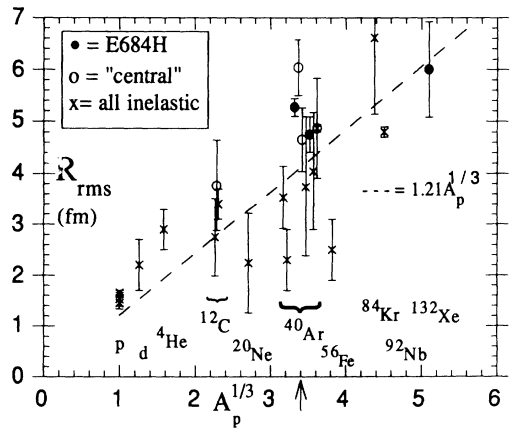

FIG. 15. Comparison with results of others. The dashed line represents the "effective nuclear radius." Filled circles are data from this experiment.

what Bartke refers to as the "effective nuclear radius" and was derived from a series of inelastic (interaction) cross section measurements for various nuclei [32]. The data points for carbon and argon have been spread out a bit to separate the points. The arrow on the x axis points to the appropriate position for argon. The data points appear to exhibit a scaling with $A_p^{1/3}$.

As shown earlier, the extracted pion source shapes do not appear to be spherical; thus, it is interesting to compare the source shapes with those measured by others. There are only five results that we are aware of in nucleus-nucleus collisions where the shape of the source has been investigated. Beavis and the Riverside group [29] extracted a spherical source shape for 1.5A GeV argon on KCl in their studies using the LBL streamer chamber. Within their uncertainties, however ($R_\perp = 5.03 \pm 0.47$ fm, $R_\parallel = 5.11 \pm 1.17$ fm), their results agree with those presented here. The same group also investigated [25] the source shape for 1.8A GeV argon on lead and extracted radii that were spherical ($R_\perp = 5.67 \pm 0.54$ fm, $R_\parallel = 5.16 \pm 0.50$ fm) within uncertainties.

Chacon [23] *et al.* extracted an oblate source shape for 1.7A GeV Fe on Fe. More recently, the same group [24] have done a source shape analysis for 1.8A GeV argon on KCl, at 0°, using the Janus spectrometer at the BEVALAC. Their results ($R_\perp = 4.8 \pm 0.3 \pm 0.07$ fm, $R_\parallel = 4.2 \pm 0.4 \pm 0.2$ fm, $\tau = 1.1^{+1.4}_{-1.1} \pm 0.4$, $\lambda = 0.81 \pm 0.05 \pm 0.03$) agree within uncertainties with those presented here in all four fit parameters. In the same paper they give results for 1.54A GeV ^{93}Nb on Nb in which they extracted a spherical source shape.

CONCLUSIONS

The results obtained for argon on KCl are more precise than any yet published for this well studied system. The results presented here for xenon on lanthanum represent the heaviest system yet reported using pion correlations. While the results of the data set taken with the peripheral collision trigger do not allow us to make a conclusive statement about the correlation between the size of the leading projectile fragment and the extracted size of the pion source, the results are suggestive of the trend which one expects (the smaller the projectile fragment the larger the size of the pion source). The source shapes extracted are oblate for the argon on KCl and lanthanum data, and prolate for the xenon on lanthanum data, although preliminary analysis of a more precise follow-up La on La experiment suggests that this source is also oblate.

The HISS facility is well suited to pion correlation studies. The large phase space acceptance of the HISS system uncouples to a large degree the determination of the HBT fit parameters and reduces the size of any acceptance related correlations in one's background pion pair distribution.

ACKNOWLEDGMENTS

This work was supported by NSF Grant PHY87-2208, DOE Grant DE-FG03-86ER40271, and by the Director of Energy Research, Division of Nuclear Physics of the Office of High Energy and Nuclear Physics of the U.S. Department of Energy under Contract DE-AC03-76SF00098.

APPENDIX: CONVERSION FACTORS

In this appendix we briefly discuss the conversion factors which are commonly used in two-particle correlation analyses. Recall that in deriving the two-particle correlation function one finds that

$$C_2(q,q_0) = 1 + |\rho(q,q_0)|^2 ,$$

where $\rho(q,q_0)$ is the Fourier transform of the pion emitting source distribution. At this point one must choose a distribution for $\rho(\mathbf{r},t)$. In Yano and Koonin's formulation [11], which we have used in this analysis, a Gaussian distribution was chosen which was parametrized as

$$\rho_1(r)d\mathbf{r} \propto ce^{(-r^2/R^2)}d\mathbf{r} .$$

In this discussion we ignore the time component of the distributions for simplicity. This leads to a correlation function of the form

$$C_2(q,q_0) = 1 + e^{-q^2R^2/2} .$$

When one fits this function to the data and quotes a radius parameter, the quantity being quoted is thus this parameter R, which is dependent on how one chooses to parametrize the Gaussian function.

The trouble that arises is that different theoretical formulations have used different algebraic forms for their Gaussians and hence one must be careful when comparing the quoted radius parameters from different groups. As an example, some formulations parametrize their Gaussians as

$$\rho_2(r)d\mathbf{r} \propto ce^{-r^2/2R^2}d\mathbf{r} .$$

This leads to a correlation function of the form

$$C_2(q,q_0) = 1 + e^{-q^2R^2} .$$

One may easily see that the extracted radius parameters for the two Gaussian parametrizations given above will differ by a factor of $\sqrt{2}$. Recognizing this problem, Bartke and Kowalski [33] suggested that if the results are quoted using the root-mean-square (rms) radii of the Gaussians this ambiguity can be avoided. This is illustrated below.

Using ρ_1 above,

$$\frac{\int_0^\infty r^2\rho_{(1)}(r)d\mathbf{r}}{\int_0^\infty \rho_1(r)d\mathbf{r}} = \frac{4\pi c\int_0^\infty r^4 e^{-r^2/R^2}dr}{4\pi c\int_0^\infty r^2 e^{-r^2/R^2}dr} = \frac{3R^2}{2} = \langle r^2 \rangle \quad \therefore r_{\rm rms} = \sqrt{\tfrac{3}{2}}R_1 .$$

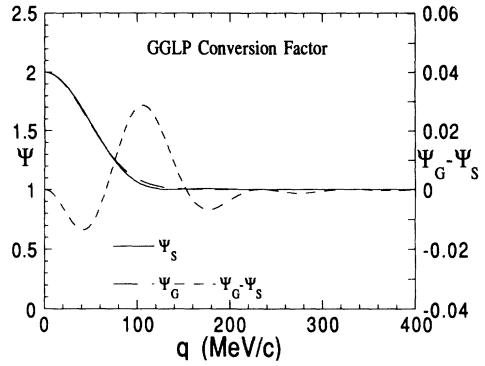

FIG. 16. The long dashed line represents correlation function using a Gaussian source distribution. The solid line is for a spherical source distribution with a radius equal to 1.52 times the Gaussian radius parameter. The short dashed line is the percentage difference between the two as read off the scale to the right.

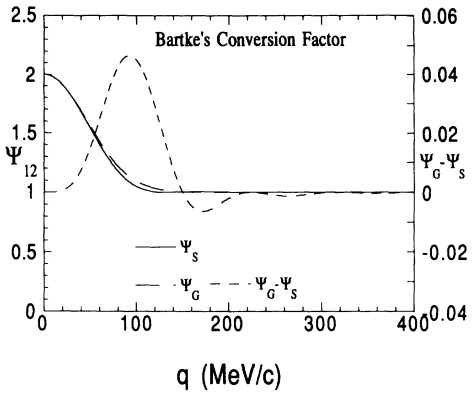

FIG. 17. Bartke's conversion factor. Same quantities as those plotted in Fig. 16 (see Fig. 16 caption) with spherical radius parameter equal $\sqrt{\frac{5}{2}}$ times the Gaussian radius parameter.

Using ρ_2 above,

$$\frac{\int_0^\infty r^2\rho_2(r)d\mathbf{r}}{\int_0^\infty \rho_2(r)d\mathbf{r}}=\frac{4\pi c\int_0^\infty r^4 e^{-r^2/2R^2}dr}{4\pi c\int_0^\infty r^2 e^{-r^2/2R^2}dr}=3R^2=\langle r^2\rangle \quad \therefore\ r_{\rm rms}=\sqrt{3}R_2\ .$$

As we have already seen, $\sqrt{2}R_2=R_1$; therefore, two different groups could analyze the same experimental data, using the different parametrizations for their Gaussians, and get the same result if they compare their rms radii.

Bartke and Kowalski also give various conversion factors to convert the extracted radius parameters (for example, R_1 and R_2 above) to the rms radii for an equivalent sharp sphere with the pion emitters distributed uniformly inside. These conversion factors are calculated by equating the rms radii of the Gaussian distributions with those for a uniform sphere, as illustrated below.

For a uniform spherical distribution

$$\frac{\int_0^{R_u} r^2 d\mathbf{r}}{\int_0^{R_u} d\mathbf{r}}=\frac{4\pi\int_0^{R_u} r^4 dr}{4\pi\int_0^{R_u} r^2 dr}=\frac{3R_u^2}{5}=\langle r^2\rangle_u \quad \therefore\ r_{\rm rms}=\sqrt{\tfrac{3}{5}}R_u\ .$$

Equating this to the rms radius for ρ_1 above,

$$\sqrt{\tfrac{3}{5}}R_u=\sqrt{\tfrac{3}{2}}R_1 \quad \therefore\ R_u=\sqrt{\tfrac{5}{2}}R_1\ .$$

The conversion factors which Bartke and Kowalski have tabulated for converting to the rms radii for the various Gaussian parametrizations are correct and applicable to two-particle interferometry analyses. We do not believe the same can be said for their conversions to uniform spheres. The factors are correct but they are not applicable to two-particle interferometry analyses [34]. The problem lies in the fact that it is the Fourier transform of the Gaussian and the uniform spherical distributions between which one wants to convert. Goldhaber, Goldhbar, Lee, and Pais [14] showed in their pioneering paper that the Fourier transform of a Gaussian and a uniform spherical distribution are almost identical (within $\approx 2\%$ everywhere) if one multiplies the width parameter for the Gaussian by the appropriate constant.

Figure 16 shows the two-pion correlation function derived using a uniform spherical distribution (Ψ_S), the same function derived using a Gaussian distribution (Ψ_G), and the difference between the two ($\Psi_G-\Psi_S$). In the plot we have used Ψ instead of $C2(q)$ to be consistent with GGLP's notation. In Fig. 17 we show the same plot where we have used the conversion factor between the Gaussian and spherical distributions given by Bartke and Kowalski [33].

It is clear from the comparison of Figs. 16 and 17 that the deviation between the correlation functions which one derives using the uniform spherical and Gaussian distributions of pion emitters is smaller when one applies GGLP's conversion factor.

From GGLP's paper the appropriate conversion factor between the Gaussian and the uniform sphere is 1.52 if one uses the Yano-Koonin formulation (ρ_1), and 2.15 if one uses a Gaussian parametrization of type ρ_2.

[1] S. Nagamiya, Univeristy of Tokyo Report No. UTPN-186; S. Nagamiya, in *Proceedings of the 3rd International Conference on Ultra Relativistic Nucleus-Nucleus Collisions,* Brookhaven National Laboratory, 1983, edited by T. W. Ludlam and H. E. Wegner (North-Holland, Amsterdam, 1984).
[2] J. Hufner, K. Schafer, and B. Schurmann, Phys. Rev. C **12**, 1888 (1975).
[3] D. J. Morrissey, W. R. Marsh, R. J. Otto, W. Loveland, and G. T. Seaborg, Phys. Rev. C **18**, 1267 (1978).
[4] L. F. Oliveira, R. Donangelo, and J. O. Rasmussen, Phys. Rev. C **19**, 826 (1979).
[5] R. Hanbury-Brown and R. Q. Twiss, Nature **178**, 1046 (1956).
[6] E. V. Shuryak, Phys. Lett. **44B**, 387 (1973).
[7] G. I. Kopylov and M. I. Podgoretskii, Yad. Fiz. **18**, 656 (1974) [Sov. J. Nucl. Phys. **18**, 336 (1974)].
[8] G. Cocconi, Phys. Lett. **49B**, 459 (1974).
[9] S. E. Koonin, Phys. Lett. **70B**, 43 (1977).
[10] F. B. Yano and S. E. Koonin, Phys. Lett. **78B**, 556 (1978).
[11] M. Gyulassy, S. K. Kauffman, and L. W. Wilson, Phys. Rev. C **20**, 2267 (1979).
[12] W. J. Knox, Phys. Rev. D **10**, 65 (1974).
[13] W. B. Christie, Ph.D. thesis, University of California, Davis, reproduced as LBL Report No. 28986, 1990.
[14] G. Goldhaber, S. Goldhaber, W. Lee, and A. Pais, Phys. Rev. **120**, 300 (1960).
[15] W. A. Zajc, Ph.D. thesis, University of California, Berkeley, LBL Report No. 14864, 1982; W. A. Zajc *et al.,* Phys. Rev. C **29**, 2173 (1984); W. A. Zajc, Nevis Laboratory Report No. 1384, Columbia University.
[16] M. Deutchmann, *et al.,* CERN Report No. CERN/EP/Phys 78-1, 1978.
[17] M. Gyulassy, Phys. Rev. Lett. **48**, 454 (1982).
[18] J. Engelage *et al.,* Nucl. Instrum. Methods **A277**, 431 (1989).
[19] Description of smaller prototype, T. Kobayashi, F. S. Bieser, P. J. Lindstrom, T. J. M. Symons, D. E. Greiner, and H. J. Crawford, Nucl. Instrum. Methods **A254**, 281 (1987).
[20] A. Shor *et al.,* Phys. Rev. Lett. **63**, 2192 (1989).
[21] D. Beavis, S. Y. Chu, S. Y. Fung, W. Gorn, D. Keane, R. Poe, G. VanDalen, and M. Vient, Phys. Rev. C **28**, 2561 (1983).
[22] J. P. Sullivan *et al.,* Phys. Rev. C **25**, 1499 (1982).
[23] A. D. Chacon *et al.,* Phys. Rev. C **60**, 780 (1988).
[24] A. D. Chacon *et al.*, Phys. Rev. C **43**, 2670 (1991); A. D. Chacon, Ph.D. thesis, University of California, Berkeley, reproduced as LBL Report No. 28149, 1989.
[25] D. Beavis, S. Y. Chu, S. Y. Fung, D. Keane, Y. M. Liu, G. VanDalen, and M. Vient, Phys. Rev. C **34**, 757 (1986).
[26] Stuart L. Wilson, *Data Analysis for Scientists and Engineers* (Wiley, New York, 1975).
[27] D. Beavis, S. Y. Fung, W. Gorn, A. Huie, D. Keane, J. J. Lu, R. Poe, B. Shen, and G. VanDalen, Phys. Rev. C **27**, 910 (1983).
[28] S. Pratt, Phys. Rev. Lett. **53**, 1219 (1984).
[29] P. J. Siemens and J. O. Rasmussen, Phys. Rev. Lett. **42**, 880 (1979).
[30] S. Nagamiya, M. C. Lemaire, E. Moeller, S. Schnetzer, G. Shapiro, H. Steiner, and I. Tanihata, Phys. Rev. C **24**, 971 (1981).
[31] J. Bartke, Phys. Lett. B **174**, 32 (1986).
[32] I. Tanihata, *Proceedings of the 7th High Energy Heavy Ion Study, Darmstadt, 1984,* Report No. GSI-85-10, Darmstadt, 1985, p. 413.
[33] J. Bartke and M. Kowalski, Phys. Rev. C **30**, 1341 (1984).
[34] Y. Z. Jiang *et al.,* Phys. Rev. C **44**, 1957 (1991).

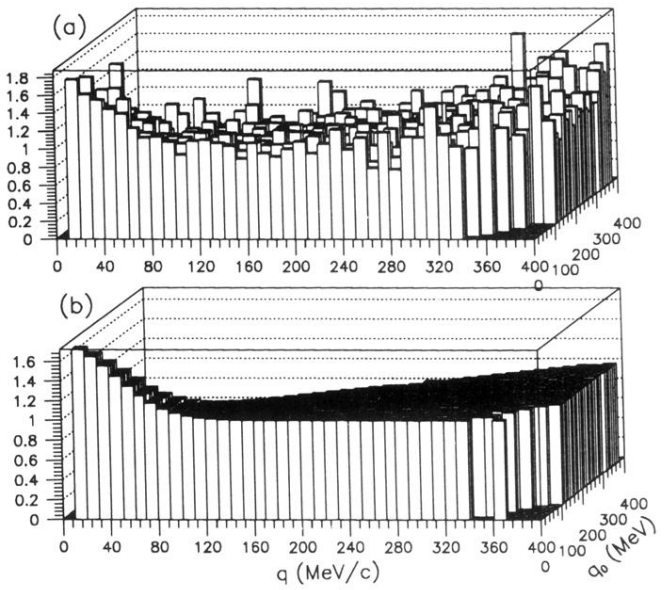

FIG. 6. $C(q,q_0)$ vs q and q_0 for Ar on KCl, hard trigger data set. (a) The experimental correlation data and (b) the fit. The DC efficiency and Gamow corrections are applied.